

Performance of novel CaO-based sorbents in high temperature CO₂ capture under RF heating

Maria Sotenko^a, Javier Fernández^a, Guannan Hu^a, Vladimir Derevschikov^{b,c}, Anton Lysikov^{b,c}, Ekaterina Parkhomchuk^{b,c}, Victoria Semeykina^{b,c}, Alexey Okunev^{b,c}, Evgeny V. Rebrov^{a,d,*}

^a School of Engineering, University of Warwick, Coventry CV4 7AL, UK

^b Boreskov Institute of Catalysis, pr. Lavrentieva 5, Novosibirsk, 630090, Russia

^c Novosibirsk State University, Novosibirsk, 630090, Russia

^d Department of Biotechnology and Chemistry, Tver State Technical University, A. Nikitina st., 22, Tver, 170026, Russia

* E-mail: E.Rebrov@warwick.ac.uk

Abstract

The problem of CO₂ mitigation on a small and medium scale can be resolved by developing a combined system of CO₂ capture and its consecutive conversion into valuable products. The first stage of CO₂ looping, however, should be reliable, effective and easy to control and radiofrequency heating, as a new advanced technology, can be used to improve the process. CO₂ absorption and desorption RF units can be installed within power plants and powered during the periods of low energy demand thus stabilizing the electrical grid. In this work, a CaO sorbent produced by template synthesis was studied as a sorbent for a CO₂ looping system under RF heating which offers short start-up times, highly controlled operation, high degree of robustness and low price. The sorbent reached its stable CO₂ capacity of 15.4 wt.% already after 10 temperature cycles (650/850 °C) under RF heating. Higher CO₂ desorption rate and lower degree of the sorbent sintering was observed under RF heating as compared to conventional heating.

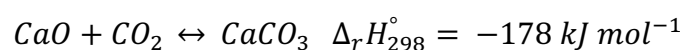
Keywords: CaO, CO₂ looping; sintering; RF heating

1. Introduction

The problem of CO₂ mitigation still causes serious concerns among different stakeholders and participants, such as public, environmental scientists, businessmen, and government and legislation agencies. As high as 80-95 % reduction in total CO₂ emissions has been put by the Committee on Climate Change as a major target to be achieved by the year 2050 [1]. The main contributors to the CO₂ emissions, such as power plants and transport, which could emit as high as 500-800 gCO₂/kW (gas and oil power plant, for example), are put under enormous pressure for developing and adopting various CO₂ capture technologies [2]. The main requirements for such a technology are high efficiency, low installation and maintenance costs, robustness and prolonged life cycle.

In general, CO₂ capture and storage, CCS, has been proposed as a useful approach for CO₂ [3,4]. Reverse absorptive methods are in this category and they can use either liquid (amine based solutions, for example) [5] or solid sorbents [6–9] in order to selectively capture emitted CO₂ with the following desorption stage. In comparison to solvent scrubbing methods which require construction of spacious facilities and tanks to handle great quantities of amine-based solvents, solid oxide based reverse absorption methods are considered to be cost-effective alternative for the problem of CO₂ mitigation. The technology of CaO looping is rapidly developing and its application in fluidised bed reactors has been extensively studied over the past few years on a pilot scale [10–13].

CaO as a solid sorbent for CO₂ has been well studied in the calcium looping cycle and offers some benefits, such as cheap precursors and simplicity of the preparation procedure, high stability and absorption capacity [14–19]. The theoretical absorption capacity of CaO is 79 wt. % following the reaction:



The CaO looping cycle consists of two stages: carbonation and calcination. In the carbonation stage, CaO absorbs CO₂ at 650-680 °C to form calcium carbonate. This temperature interval makes CaO-based materials a suitable sorbent for the treatment of hot post-combustion gases. The calcination step is usually performed in the range of 850-950 °C. The exposure to high temperature causes sintering of the CaO-based sorbents with time which eventually leads to significant loss in absorption capacity. The effect of loss-in-capacity over several cycles was found to be common for different types of CaO sorbents regardless of the type of the limestone precursor used for their synthesis [20]. This effect is considered to be the main hurdle in wider application of this sorbent and has been intensively studied.

It was observed that the grain size has a profound effect on the thermal stability of the sorbent with smaller grains being responsible for faster sintering [21]. Doping of CaO with small cations, for example Al³⁺, or supporting it onto a thermostable support (such as alumina) could reduce the sintering kinetics [22,23]. Other doping elements (Zr, La, Mg) have been also studied [24]. New types of CaO based sorbents with unique cage-like spherical structure demonstrated theoretical CO₂ capacity [25–27]. A template approach using polymeric microspheres provided CaO sorbents with enhanced recarbonation/decomposition performance due to their high total pore volume [28]. Thus, the sorbent stability can be substantially improved by chemical modification and/or by modification of its porous structure and grain size. Also, the choice of the precursor [29] and the granules abrasion in fluidised bed reactors [30] was found to influence the stability. It was also reported that irregular heating regimes and localised overheating could accelerate the sorbent sintering in fixed bed reactors [20].

The problem of localised overheating can be resolved by using precise temperature control during temperature transitions under radiofrequency (RF) heating [31]. Although currently

rarely used on a large scale, RF heating has a great potential to become highly competitive heating method in the near future. One of the main advantages of RF heating is its high efficiency within 65 - 85 % in comparison to only 55 % for conventional (transient) operation methods [32]. The technology has proved to be highly efficient with low installation costs when first was used by DuPont researchers for a continuous production of hydrogen cyanide over a Pt group metal catalyst at 1000 °C [33]. Nowadays due to its high efficiency, safety and fast heating times [34,35], the RF heating technology, is increasingly being used in various industries, such as in metallurgy, in civil and medical applications, melting technology, hypothermia and many others [36].

In this paper we studied the sintering behavior of two optimized CaO sorbents prepared via template synthesis [28]. The effect of precise temperature control onto the sorbents dynamic capacity and the structural changes has been studied.

2. Experimental

2.1 Materials

The CaO sorbents were prepared using template synthesis. Template beads were produced using emulsifier-free emulsion polymerization method at 90 °C as described in [37]. The obtained polystyrene (PS) spheres were isolated from the reaction mixture by centrifugation, washed with ethanol and dried in air until constant weight. The average size of the synthesized polystyrene beads was confirmed by SEM analysis.

The CaO sorbents were prepared by the technique described in details elsewhere [28]. The precursor for the CaO sorbent was obtained from the micron sized CaCO₃ powder (99 wt.%, ReaChem, Russia) which was heated in air at 900 °C for 3 h in an oven. The product was ground in a mortar and carefully mixed with the PS spheres. The PS beads were mixed with CaO in desired ratio to obtain a template loading of 20 and 40 wt.%. A ductile paste was

prepared by addition of a water-ethanol solution under vigorous stirring and grinding in a mortar. The paste was extruded using a plunger extruder equipped with a 3 mm extrusion die. The extrudates were cut into equal parts, and obtained pellets were calcined at 900 °C for 3 h. Two sorbents with a loading of 20 and 40 wt.% of polystyrene template will be referred to as S-20 and S-40 hereafter. Despite very small size of the template particles of 180 nm, the final pores diameters in the CaO particles appeared to be much higher (> 300 nm) and within a broader range of sizes due to strong particle agglomeration that occurs during the polymer evaporation stage. This morphology provides high surface area and large inter porous spacing resulting in better sorption capacity for CO₂ over prolonged periods of time.

2.2 Reactor set-up

The CaO sorbent (400 mg, 300-600 µm fraction) was positioned in the center of the Inconel reactor (6.0 mm i.d., 7.0 mm o.d., 250 mm length, Corrotherm international) between two layers of SiC particles of the same size which were used for thermal insulation. The reactor was placed inside a 4-turn RF coil connected to an RF-generator (Easyheat Ambrell). An alumina tube (10 mm i.d., 16 mm o.d., Almath crucibles) was used as insulation. A 10 mm circular opening in the alumina tube allowed to measure the temperature on the surface of the inconel tube by a FLIR A655sc infrared camera. A tubular quartz reactor (8 mm i.d., 10 mm o.d.) was used in the experiments under conventional heating. The heating was provided by a electrical heating jacket and the temperature was monitored at the surface of the sorbent bed by a thermocouple. Both reactors [31] were able to operate with direct and reverse flow of N₂ in desorption mode relative to that in the absorption mode. The CO₂ concentration was continuously measured at the outlet by a mass spectrometer (Pfeiffer GSD 320 O3) and an IR CO₂ detector (Dynamment).

The following procedure was followed for a single CO₂ absorption/desorption cycle: the reactor was flushed with N₂ and then preheated to 650 °C. After temperature stabilization, a mixture

of 30 vol. % CO₂ in N₂ was fed to the reactor at a flow rate of 10 mL/min (STP). Once the CO₂ concentration started to increase, the CO₂ flow was stopped and the temperature was raised to 850 °C to start the CO₂ desorption. The experiments were stopped when no more changes (within the experimental error) in the dynamic capacity was observed in five consecutive cycles. The dynamic sorption capacity is determined as kg of CO₂ absorbed per kg sorbent and expressed in wt. %.

2.3 Sorbent characterization

The morphology of the sorbents was studied before and after CO₂ absorption with SEM using a Zeiss Sigma microscope (Carl Zeiss Ltd., Welwyn Garden City, UK) operated at 2 kV. The samples were mounted on a sample holder with a double sided carbon tape and coated with a carbon layer (40 sec, 15 nm estimated coating thickness) using a K450X Carbon Coater (Quorum Technologies, UK). Nitrogen adsorption isotherms before and after the experiments were obtained at -196 °C using a Micromeritics ASAP2020 apparatus. The specific surface area was calculated from the N₂ adsorption data according to the Brunauer-Emmett-Teller (BET) method using P/P₀ values in the range of 0.05–0.20. XRD analysis of the samples was carried out using a PANalytical Empyrean X-Ray Diffractometer with CoK α radiation ($\lambda = 1.78901 \text{ \AA}$) at 45 kV and 40 mA in the 5-75 ° range of 2 θ .

3. Results

3.1 Temperature profiles

Conventional heating with electric current is a common method for heating bench scale reactors. Such heating however cannot provide uniform heat flux along the length of the tube and leads to localized hot-spots or cold zones. Due to large thermal inertia of the reactor, it is

difficult to provide near-isothermal conditions during absorption and desorption cycles under conventional heating (Figure 1a). The rather large thermal inertia leads to overheating of the reactor by 20 °C. The heating requires a slow approach to the set-point which takes about 6 min. The cooling part of the cycle requires ca. 10 min and a constant overshoot to lower temperature by 17 °C is observed. The overall heat transfer coefficient determines the heating and cooling rates with the highest thermal resistance in the boundary layer between the hot air around the reactor and the reactor wall. A large thermal gradient of around 60 °C between the oven and the reactor is required. This requires several optimisation cycles to improve the temperature control loop in the conventional reactor. Yet, a simple PID controller could not provide a near-isothermal behaviour and a more advance control mechanism (such as feed forward) is needed to reduce the temperature overshoot in both heating and cooling cycles without increasing the cycle time.

However under RF heating (Figure 1b), none of the above mentioned problems have been observed, so that the step change in temperature was accurate, there was no time lag, and no overshoot to higher or lower temperatures was noticed. Small temperature oscillations of 0.5 °C around the set-point were observed under RF heating. However they are considered to be insignificant in comparison to the reactor performance under conventional heating. Thus RF heating has proved to be a precise and accurate method of heating with fully reproducible temperature cycles.

A typical absorption/desorption cycle is 25 min under RF heating. This extends to 40 min under conventional heating due to much slower transient steps of heating and cooling according to the temperature profiles depicted in Figure 1. It has been also proved that the RF heating mode reduces the heat loss by 4 times [31].

Insert Figure 1 here

Two typical absorption-desorption cycles under conventional and RF heating are shown in Figure 2. During the first few minutes, when CO₂ is absorbed by CaO at 650 °C, a zero CO₂ signal is observed in the outlet mixture. Here, two regions can be seen: (i) fast absorption as the result of the reaction of CaO with CO₂ and then (ii) slower absorption hindered by the CO₂ diffusion through the CaCO₃ layer on the surface of CaO [8,38]. Close to the total CO₂ capacity of the sorbent, the outlet CO₂ concentration starts to increase and finally levels off at the value corresponding to its inlet concentration. Then, the flow of CO₂ is stopped and the temperature increases to 850°C. An asymmetric peak of the desorbed CO₂ is observed at this stage corresponding to the decomposition of CaCO₃.

The absorption and desorption stages yielded similar patterns with some minor differences under RF and conventional heating. The desorption peak is characterised by an extended tail which corresponds to a stage when slower desorption is observed due to diffusion limitations. Firstly, CO₂ desorbs from the surface of the CaCO₃ grains. In this case, the desorption rate is determined solely by the reaction rate of CaCO₃ decomposition. Secondly, CO₂ desorbs from the inner layers of the grains but the desorption rate at this stage is reduced by slow diffusion of the CO₂ from the core to the surface of the grain. As the result, the desorption peak is highly asymmetric in both heating methods. However, somewhat prolonged CO₂ desorption observed under conventional heating. The amount of CO₂ in the tail part of the desorption peak obtained in the first two absorption-desorption cycles is listed in Table 1. This increases the duration of cycle under conventional heating.

The initial desorption rate of 14.3 vol.% CO₂ min⁻¹ was a factor of 2.7 higher under RF-heating as compared with conventional heating. Shorter heating time under RF heating allows to reduce the total duration of the cycle by 7 %.

Insert Figure 2 here

Insert Table 1 here

3.2 Study of CO₂ dynamic sorption capacities under RF and conventional heating

A CaO sorbent without using the PS spheres was prepared and its properties have been described in Ref [28]. Briefly, the macroporous structure formed after the template removal significantly increases the rate of both recarbonation and decomposition reactions. The decomposition rate of the sorbent produced from a 40% templated composite was an order of magnitude higher than the rate of a reference sample produced in the absence of the template. Therefore the non-templated sample was not studied in the present work. Figure 3 shows the comparison between the dynamic capacity of the S-20 and S-40 sorbents under RF and conventional heating. Firstly, a similar total capacity for both samples was observed which indicates that both sorbents behave uniformly regardless of the heating mode. However, a significant difference was observed for the time to reach the equilibrium capacity. Under RF heating, the samples achieved the equilibrium capacity within 15 cycles in comparison to as many as 40 cycles required under conventional heating. Time wise, the difference amounts to more than 6 hours between RF and conventional heating. On a large scale this would correspond to a one operator shift difference between the two regimes demonstrating higher monetary and time benefits of the RF heating mode.

Insert Figure 3 here

Under conventional heating, the sorption capacity of S-20 was higher than that of S-40 (14.2 and 11.0 wt.%, respectively, see Figures 3 a and b). However under RF-heating, the sorption capacity (based on the amount of CO₂ absorbed) of S-20 was lower than that of S-40 (10.9 and

15.5 wt.% CO₂ respectively, see Figures 3 c and d). The final dynamic capacity of both samples decreases by ca 2 wt.% when calculated from the desorption signal.

Overall, S-40 sample performed better in comparison to S-20 under RF heating. Thus, the final capacity of S-40 was higher. The stabilization time over S-40 was 10 cycles as compared to 15 cycles for S-20, mainly due to different initial morphology of these samples.

The XRD patterns showed that the CaO core is covered with a layer of portlandite (calcium hydroxide) to the depth of the X-ray penetration (< 200 μm) in both S-20 and S-40. Its characteristic peaks can be observed at 18.1, 28.7, 34.2, 47.2 and 54.6° 2-theta corresponding to (001), (100), (101), (102) and (111) planes, respectively (Figure 4a, b). The portlandite layer is formed by the interaction of CaO with water vapour present in the air [27, 39]. The portlandite layer is present onto the surface of the CaO pellets as thin interconnected grains as confirmed by the SEM image of S-40 (Figure 5a). The XRD peaks of portlandite are broader indicating that its crystallite size is smaller as compared to that of CaO. The S-40 sample demonstrated an XRD pattern which is characteristic of CaO with less than 30 wt.% calcium hydroxide (Figure 4b). The S-20 sample, however, demonstrated much greater coverage with calcium hydroxide (no CaO XRD peaks were observed to the depth of the analysis) and this higher initial coverage of S-20 with portlandite contributed to lower dynamic CO₂ capacity.

After the CO₂ absorption, both samples were converted to CaCO₃ (calcite) according to the obtained XRD patterns (Figure 4). However the presence of minor amounts of non-converted portlandite phase can be seen in both samples.

Insert Figures 4 and 5 here

The S-40 sample is characterised by somewhat higher pore size and total porosity (Table 2) [28] and, although the initial surface area for both samples is quite similar, higher voidage

secured better performance of the S-40 sample under fast heating regime. Moreover, under fast RF-heating, the sintering of S-40 is less pronounced therefore it reaches the equilibrium capacity much faster and it retains much higher CO₂ sorption capacity. After 20 absorption cycles, the specific surface area of S-20 and S-40 reduced by 54 and 10%, respectively (Table 2). Thus, the S-40 sorbent with higher porosity retains most of its initial porosity.

Insert Table 2 here

In addition, higher content of Ca(OH)₂ on the surface of the S-20 sample also contributed to its inferior performance. Portlandite was reported to demonstrate similar to CaO or higher carbonation extent and somewhat faster CO₂ absorption kinetics [40,41]. However, according to the obtained results small grains of Ca(OH)₂ are more prone to sintering at high temperatures which eventually leads to the reduction in the CO₂ absorption efficiency.

4. Conclusions

The sintering behavior of two CaO sorbents, prepared by template synthesis using emulsifier-free emulsion polymerization method, has been compared under RF and conventional heating when absorbing CO₂ from a 30 vol.% CO₂/N₂ mixture at 650 °C followed by its desorption at 850 °C. The sorbent prepared with a template loading of 40 wt.% demonstrated lower surface area and higher average pore size as compared to the sorbent prepared with a 20 wt.% template loading. Shorter cycle and start-up times, highly controlled operation without temperature overshoots was observed under RF heating during both absorption and desorption. The sorbent reached its stable operation already after 10 absorption/desorption cycles under RF heating as compared to 35 cycles under conventional heating. The initial CO₂ desorption rate was also increased a factor of 2.7 and a higher dynamic CO₂ capacity of 15.4 % g CO₂ per g of CaO

was observed under RF-heating for the sorbent with lower surface area. However under conventional heating, the sorbent with higher surface area (template loading of 20 wt.%) demonstrated a better performance, however its equilibrium dynamic CO₂ capacity of 14.2 % g CO₂ per g of CaO was lower.

5. Acknowledgements

The financial support provided by the Russian Science Foundation (project 15-13-20015) is gratefully acknowledged.

References

- [1] Commette on Climate Change, Climate Change Act 2008, Station. Off. Ltd. 27 (2008) 1–102.
- [2] J.G.J. Olivier, G. Janssens-Maenhout, M. Muntean, J.A.H.W. Peters, Trends in global CO₂ emissions: 2014 report, PBL Netherlands Environ. Assess. Agency, Hague, Netherlands. (2014) 1–60.
- [3] S. Anderson, R. Newell, Prospects for carbon capture and storage technologies, Discuss. Pap. (2003) 1–67.
- [4] R. Golombek, M. Greaker, A.C. Sverre, Carbon capture and storage technologies in the European power market, Discuss. Pap. (2009) 1–29.
- [5] B. Dutcher, M. Fan, A.G. Russell, Amine-Based CO₂ Capture Technology Development from the Beginning of 2013: A Review, Appl. Mater. Interfaces. 7 (2015) 2137–2148. doi:10.1021/am507465f.
- [6] B. Dou, C. Wang, Y. Song, H. Chen, B. Jiang, M. Yang, Y. Xu, Solid sorbents for in-situ CO₂ removal during sorption-enhanced steam reforming process : A review, Renew. Sustain. Energy Rev. 53 (2016) 536–546. doi:10.1016/j.rser.2015.08.068.
- [7] G. Bhatta, S. Subramanyam, M.D. Chengala, S. Olivera, K. Venkatesh, Progress in hydrotalcite like compounds and metal-based oxides for CO₂ capture: a review, J. Clean. Prod. 103 (2015) 171–196. doi:10.1016/j.jclepro.2014.12.059.
- [8] M. Erans, V. Manovic, E.J. Anthony, Calcium looping sorbents for CO₂ capture, Appl. Energy. 180 (2016) 722–742. doi:10.1016/j.apenergy.2016.07.074.

- [9] J. Adanez, A. Abad, F. Garcia-labiano, P. Gayan, L.F. De Diego, Progress in Chemical-Looping Combustion and Reforming technologies, *Prog. Energy Combust. Sci.* 38 (2012) 215–282. doi:10.1016/j.pecs.2011.09.001.
- [10] B. Arias, M. Alonso, C. Abanades, CO₂ Capture by calcium looping at relevant conditions for cement plants: experimental testing in a 30 kW pilot plant, *Ind. Eng. Chem. Res.* in press (2017). doi:10.1021/acs.iecr.6b04617.
- [11] M.E. Diego, B. Arias, A. Méndez, M. Lorenzo, L. Díaz, A. Sánchez-biezma, J.C. Abanades, Experimental testing of a sorbent reactivation process in La Pereda 1.7 MWth calcium looping pilot plant, *Int. J. Greenh. Gas Control.* 50 (2016) 14–22. doi:10.1016/j.ijggc.2016.04.008.
- [12] M.E. Diego, B. Arias, J.C. Abanades, Analysis of a double calcium loop process configuration for CO₂ capture in cement plants, *J. Clean. Prod.* 117 (2016) 110–121. doi:10.1016/j.jclepro.2016.01.027.
- [13] M.C. Romano, I. Martínez, R. Murillo, B. Arstad, R. Blom, D. Can, H. Ahn, S. Brandani, Process simulation of Ca-looping processes: review and guidelines, *Energy Procedia.* 37 (2013) 142–150. doi:10.1016/j.egypro.2013.05.095.
- [14] J. Udomsirichakorn, P.A. Salam, Review of hydrogen-enriched gas production from steam gasification of biomass : The prospect of CaO-based chemical looping gasification, *Renew. Sustain. Energy Rev.* 30 (2014) 565–579. doi:10.1016/j.rser.2013.10.013.
- [15] A. Sánchez-Biezma, J.C. Ballesteros, L. Diaz, E. De Zárraga, F.J. Álvarez, J. López, Postcombustion CO₂ capture with CaO. Status of the technology and next steps towards large scale demonstration., *Energy Procedia.* 4 (2011) 852–859.

doi:10.1016/j.egypro.2011.01.129.

- [16] M.S. Yancheshmeh, H.R. Radfarnia, M.C. Iliuta, High temperature CO₂ sorbents and their application for hydrogen production by sorption enhanced steam reforming process, *Chem. Eng. J.* 283 (2016) 420–444. doi:10.1016/j.cej.2015.06.060.
- [17] L. Di Felice, CO₂ Capture by CaO-Based Sorbents and Sorption Enhanced Reaction Systems, Elsevier B.V., 2013. doi:10.1016/B978-0-444-53882-6.00022-X.
- [18] V.S. Derevschikov, A.I. Lysikov, A.G. Okunev, Sorption properties of lithium carbonate doped CaO and its performance in sorption enhanced methane reforming, *Chem. Eng. Sci.* 66 (2011) 3030–3038. doi:10.1016/j.ces.2011.04.008.
- [19] A.I. Lysikov, S.N. Trukhan, A.G. Okunev, Sorption enhanced hydrocarbons reforming for fuel cell powered generators, *Int. J. Hydrogen Energy.* 33 (2008) 3061–3066. doi:10.1016/j.ijhydene.2008.03.041.
- [20] G.S. Grasa, J.C. Abanades, CO₂ Capture Capacity of CaO in Long Series of Carbonation / Calcination Cycles, *Ind. Eng. Chem. Res.* 45 (2006) 8846–8851.
- [21] A.I. Lysikov, A.N. Salanov, A.G. Okunev, Change of CO₂ Carrying Capacity of CaO in Isothermal Recarbonation - Decomposition Cycles, *Ind. Eng. Chem. Res.* 46 (2007) 4633–4638.
- [22] D.T. Beruto, R. Botter, A. Lagazzo, E. Finocchio, Calcium oxides for CO₂ capture obtained from the thermal decomposition of CaCO₃ particles coprecipitated with Al³⁺ ions, *J. Eur. Ceram. Soc.* 32 (2012) 307–315. doi:10.1016/j.jeurceramsoc.2011.08.022.
- [23] B. Feng, W. Liu, X. Li, H. An, Overcoming the Problem of Loss-in-Capacity of

- Calcium Oxide in CO₂ Capture, *Energy & Fuels*. (2006) 2417–2420.
- [24] A. Antzara, E. Heracleous, A.A. Lemonidou, Development of CaO-based mixed oxides as stable sorbents for post-combustion CO₂ capture via carbonate looping, *Energy Procedia*. 63 (2014) 2160–2169. doi:10.1016/j.egypro.2014.11.235.
- [25] H. Ping, S. Wu, Preparation of cage-like nano-CaCO₃ hollow spheres for enhanced CO₂ sorption, *RSC Adv*. 5 (2015) 65052–65057. doi:10.1039/C5RA12251A.
- [26] S. Wang, H. Shen, S. Fan, Y. Zhao, X. Ma, J. Gong, CaO-based meshed hollow spheres for CO₂ capture, *Chem. Eng. Sci.* 135 (2015) 532–539. doi:10.1016/j.ces.2014.09.027.
- [27] M. Broda, C.R. Müller, Synthesis of Highly Efficient, Ca-Based, Al₂O₃-Stabilized, Carbon Gel-Templated CO₂ Sorbents, *Adv. Mater.* 24 (2012) 3059–3064. doi:10.1002/adma.201104787.
- [28] V. Derevschikov, V. Semeykina, J. Bitar, E. Parkhomchuk, A. Okunev, Microporous and Mesoporous Materials Template technique for synthesis of CaO-based sorbents with designed macroporous structure, *Microporous Mesoporous Mater.* 238 (2017) 56–61. doi:10.1016/j.micromeso.2016.02.032.
- [29] M. Olivares-Marín, E.M. Cuerda-Correa, A. Nieto-Sánchez, S. García, C. Pevida, S. Román, Influence of morphology, porosity and crystal structure of CaCO₃ precursors on the CO₂ capture performance of CaO-derived sorbents, *Chem. Eng. J.* 217 (2013) 71–81. doi:10.1016/j.cej.2012.11.083.
- [30] J. Blamey, E.J. Anthony, J. Wang, P.S. Fennell, The calcium looping cycle for large-scale CO₂ capture, *Prog. Energy Combust. Sci.* 36 (2010) 260–279.

doi:10.1016/j.pecs.2009.10.001.

- [31] J. Fernández, M. Sotenko, V. Derevschikov, A. Lysikov, E. V Rebrov, Chemical Engineering and Processing : Process Intensi fi cation A radiofrequency heated reactor system for post-combustion carbon capture, Chem. Eng. Process. Process Intensif. 108 (2016) 17–26. doi:10.1016/j.cep.2016.07.004.
- [32] M.H. Tavakoli, H. Karbaschi, F. Samavat, Influence of workpiece height on the induction heating process, Math. Comput. Model. 54 (2011) 50–58.
doi:10.1016/j.mcm.2011.01.033.
- [33] K.A. Kreutzer, W. Tam, Hydrocyanation process and multidentate phosphite and nickel catalyst composition, Pat. US 5512696 A. (1996) 1–21.
- [34] K.R. Krause, Catalytic oxidation of volatile carbon compounds into carbon monoxide using induction heating, 1997.
- [35] O. Bodart, R. Touzani, Numerical investigation of optimal control of induction heating processes, Appl. Math. Model. 25 (2001) 697–712.
- [36] W. Liu, M. Chen, Y. Xi, C. Lin, S. Liu, Thermo-mechanical analysis of a wafer level packaging by induction heating, Electron. Packag. Technol. High Density Packag. ICEPT-HDP 2008 Int. Conf. (2008).
- [37] E. V Parkhomchuk, K.A. Sashkina, N.A. Rudina, N.A. Kulikovskaya, V.N. Parmon, Template Synthesis of 3D Structured Macroporous Oxides and Hierarchical Zeolites, Catal. Ind. 5 (2013) 80–89. doi:10.1134/S2070050412040150.
- [38] F.N. Ridha, Y. Wu, V. Manovic, A. Macchi, E.J. Anthony, Enhanced CO₂ capture by biomass-templated Ca(OH)₂ -based pellets, Chem. Eng. J. 274 (2015) 69–75.

doi:10.1016/j.ccej.2015.03.041.

- [39] T.N. Blanton, C.L. Barnes, Quantitative analysis of calcium oxide dessicant conversion to calcium hydroxide using X-ray, *Adv. X-Ray Anal.* 48 (2005) 45–51.
- [40] G. Montes-Hernandez, R. Chiriac, F. Toche, F. Renard, Gas-solid carbonation of Ca(OH)₂ and CaO particles under non-isothermal and isothermal conditions by using a thermogravimetric analyzer : Implications for CO₂ capture, *Int. J. Greenh. Gas Control.* 11 (2012) 172–180.
- [41] S.F. Wu, T.H. Baum, J.. Yang, J.N. Kim, Properties of Ca-Base CO₂ Sorbent Using Ca(OH)₂ as Precursor, *Ind. Eng. Chem. Res.* 46 (2007) 7896–7899.

Tables

Table 1. Total amount of CO₂ desorbed under conventional and RF heating regimes.

Heating mode	Cycle	Total amount of CO ₂ desorbed (wt.%)	Amount of CO ₂ desorbed in the tail part of the desorption peak (wt.%)
Conventional	1	22.0	2.6
	2	21.7	2.2
RF	1	21.5	0.4
	2	21.3	0.3

Table 2. Surface area, pore volume and average pore size for the samples before and after the reaction.

Sample code	Surface area (m ² /g)	Pore volume (cm ³ /g)	Average pore size (nm)
S-20 fresh	28.6	0.045	4.3
S-20 spent	13.0	0.015	4.1
S-40 fresh	25.6	0.043	5.1
S-40 spent	22.9	0.037	5.4

Figure captions

Figure 1. Temperature profiles for conventional (a) and RF (b) heating regimes.

Figure 2. Two absorption/desorption cycles for conventional (a) and RF (b) heating regimes (the initial CO₂ desorption rate is represented by the gradient of the blue lines). Corresponding temperature profiles are added for clarity.

Figure 3. Dynamic absorption capacities for conventional (a, b) and RF (c, d) heating regimes for CaO samples with S-20 (a, c) and S-40 (b, d) samples.

Figure 4. XRD patterns of (a) S-20 and (b) S-40 samples before and after the absorption/desorption cycles.

Figure 5. SEM images of S-40 sample before (a) and after (b) absorption/ desorption cycles under RF heating.